



Article

On the Performance of Sentinel-3 Altimetry over High Mountain and Cascade Reservoirs Basins: Case of the Lancang and Nu River Basins

Yu Cheng ^{1,2}, Xingxing Zhang ^{1,*}  and Zhijun Yao ¹

¹ Institute of Geographic Sciences and Natural Resources Research, Chinese Academy of Sciences, Beijing 100101, China

² College of Resources and Environment, University of Chinese Academy of Sciences, Beijing 100049, China

* Correspondence: zhangxx@igsnr.ac.cn

Abstract: Satellite radar altimetry has been widely utilized in hydrological research, particularly with the advent of Sentinel-3, a Synthetic Aperture Radar (SAR) altimeter operating globally and equipped with an innovative onboard tracking system referred to as the open-loop tracking command (OLTC). Utilizing a pseudo-DEM (Digital Elevation Model), controlled through the OLTC, holds significant promise for the reliable observation of inland water bodies. Nevertheless, the complex geographical conditions in high mountain and reservoir river basins pose challenges in defining an appropriate pseudo-DEM for hydrological targets, potentially leading to reduced performance of Sentinel-3. This study aims to comprehensively evaluate the performance of Sentinel-3 by selecting the Lancang and Nu River basins in southwest China as a case study. These two rivers have a similar natural environment, but cascade reservoirs distinguish the Lancang River basin. By analyzing waveform energy from echoes of virtual stations (VSs) in both river basins (27 VSs in the Lancang River basin and 39 VSs in the Nu River basin), the performance of Sentinel-3 in different tracking modes and OLTC versions were compared. The results indicated that the detection rate of Sentinel-3A increased when transitioning from the closed-loop mode to the open-loop mode and with the implementation of newer OLTC versions (36.8% increased to 47.4%, 60.5%, and 63.2% in OLTC V5.0, V6.0, and V6.1, respectively). Similarly, the detection rate of Sentinel-3B rose from 64.3% (OLTC V2.0) to 71.4% and 75.0% in OLTC V3.0 and V3.1, respectively. Additionally, the cascade reservoir causing river channel expansion results in a better performance of Sentinel-3A in the Lancang River compared to the Nu River in the closed-loop mode (13.0% and 35.7%, respectively). Nevertheless, the considerable fluctuations in water surface caused by reservoir impoundment led to a wrong pseudo-DEM, resulting in poor performance of Sentinel-3 in reservoir regions before OLTC V6.0 was updated. The detection rate of low altitude, broad water surfaces (>500 m) decreased from 100% in a closed-loop mode to 0% in an open-loop mode, but increased to 100% in OLTC V6.0 and V6.1, respectively. The detection rate of high altitude, narrow water surfaces (<500 m) increased from 0% in a closed-loop mode to 40.9% in OLTC V6.1. Although the detection ability of Sentinel-3 is improving with the implementation of newer OLTC versions, the seasonal variations (usually more than 60 m) of water levels in reservoirs exceeded the size of the range window (60 m), rendering a complete measurement impossible.



Citation: Cheng, Y.; Zhang, X.; Yao, Z. On the Performance of Sentinel-3 Altimetry over High Mountain and Cascade Reservoirs Basins: Case of the Lancang and Nu River Basins. *Remote Sens.* **2023**, *15*, 1769. <https://doi.org/10.3390/rs15071769>

Academic Editor: Dongdong Wang

Received: 1 March 2023

Revised: 21 March 2023

Accepted: 23 March 2023

Published: 25 March 2023



Copyright: © 2023 by the authors. Licensee MDPI, Basel, Switzerland. This article is an open access article distributed under the terms and conditions of the Creative Commons Attribution (CC BY) license (<https://creativecommons.org/licenses/by/4.0/>).

Keywords: Sentinel-3A/B; water surface elevation; complex terrain; Lancang River; Nu River

1. Introduction

Water surface elevation (WSE) is a fundamental hydrological parameter that underpins a wide range of studies [1–5], including hydrodynamics characterization [6–8], flood monitoring and prediction [3,9,10], and river discharge estimation [11–14]. The impacts of climate change and human activities affect river regimes and flows [15–18], underscoring

the need for accurate WSE monitoring. However, traditional ground-based hydrological monitoring stations have limited spatial coverage, and institutional barriers can restrict data sharing [19–21]. Moreover, high mountain rivers and lakes often lack sufficient WSE data [22–24]. Thus, adopting alternative and efficient methods for collecting comprehensive regional-scale WSE data sets and making them publicly available is essential to enable better understanding and management of hydrological processes [12,25,26].

Satellite radar altimetry has emerged as a complementary tool for monitoring changes in rivers, lakes, and reservoirs [27–30], providing an accurate measurement of WSE. Although initially designed to study the ocean [31–33], satellite altimetry data have gradually been used to monitor WSE processes in large lakes and rivers with the launch of TOPEX/Poseidon and ERS-1/-2 satellites in the 1990s [30,34]. Over the past decade, satellite radar altimetry has increasingly been used to monitor terrestrial water bodies [35,36], resulting in the emergence of satellites such as CryoSat-2 and Sentinel-3. CryoSat-2, launched by the European Space Agency in 2010, is equipped with a new generation of the Synthetic Aperture Radar (SAR) altimeter [37–39]. It has an altimeter footprint of about 300 m along the orbital direction and an orbital ground separation of about 7.5 km, enabling it to detect more water bodies [33,38]. Its extended re-entry period of 369 days allows for higher measurement accuracy but makes it challenging to detect seasonal changes in water bodies, which are essential for inland water monitoring [40–42]. The SAR altimeter onboard the Sentinel-3 program, along with its binary constellation and 29-day re-entry period, has significantly improved the detection of surface water bodies [43,44], allowing for the detection of changes in land surface water levels throughout the hydrological year [45–47]. With its enhanced spatial and temporal resolution, Sentinel-3 is a valuable tool for inland water monitoring [12,25]. These advancements in satellite radar altimetry have significantly expanded our ability to collect comprehensive regional-scale data sets on WSE [48,49]. Nevertheless, satellite radar altimetry still faces challenges in areas with complex geographical conditions, such as high mountains and reservoir basins [25,26,45].

Inland water bodies are usually surrounded by rugged terrain, which can pose significant challenges to satellite signal detection [25,50,51]. To address this issue, various methods have been employed to obtain more accurate data, including the Envisat Model Free Tracker, the Jason-1 Split-gate tracker [52], the Jason-2 Diode/Median tracker [53], and the Diode/DEM tracker [51,54]. Among these, the Diode/DEM mode, also known as the open-loop tracking command (OLTC), was first tested on Jason-2 and SARAL/AltiKa missions [55,56], and demonstrated a performance improvement in sea level and wave height estimates in coastal regions compared to the closed-loop mode [51]. The open-loop mode has later been used as the operational mode for Sentinel-3 since March 2019. In a study over Chinese rivers, OLTC allowed a better tracking of water surfaces than the closed-loop mode, particularly in mountainous areas [25]. It was also pointed out that in the open-loop mode, the OLTC did not always contain the adequate elevation prior to tracking water surfaces over recently built reservoirs [26]. Moreover, the OLTC onboard Sentinel-3A (S3A for short) from V4.2 to V5.0 yielded a 30% increase in the number of water bodies over which valid water surface height could be estimated [46]. However, the OLTC table has been updated twice after OLTC V5.0, and the OLTC update can theoretically increase the detection rate of about 45% in previous study [12] to nearly 100%. However, the performance of the two updated data in mountainous, plain, and reservoir areas has not been evaluated. Therefore, studies that evaluate each change in Sentinel-3 in different topographic regions are urgently needed.

This research aims to address two questions regarding Sentinel-3. Firstly, how effective is Sentinel-3 in monitoring alpine and reservoir basins? Secondly, how do different OLTC versions and the closed-loop mode affect the quality of the data collected? Our study area is focused on the Nu and Lancang Rivers, located in southwest China. These two rivers share a similar natural environment, but the Lancang River basin features cascade reservoirs, which set it apart from the Nu River basin [14,30,57,58]. This presents a valuable opportunity for comparative analysis in this paper.

2. Materials

2.1. Study Area

Situated on the southeastern margin of the Tibetan Plateau (Figure 1), the Three Rivers region is divided into three river catchments by high mountain ridges of the Hengduan Mountains, which were formed due to the collision of India and Eurasia [59–61]. The region is characterized by the parallel watersheds of the Jinsha (upper Yangtze), Lancang (upper Mekong), and Nu (upper Salween) Rivers.

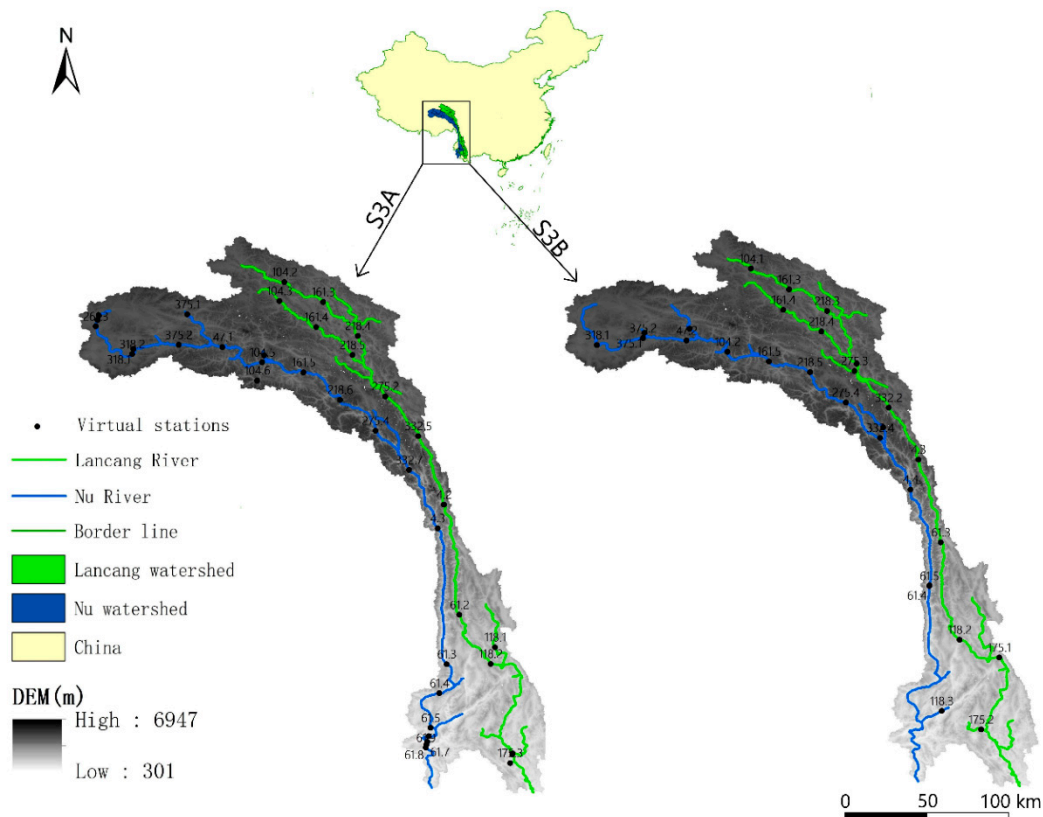


Figure 1. Base map of the study area, including DEM information of the watershed and the locations of virtual stations on major rivers. The left map shows the location and number of sentient-3A (S3A) virtual stations. The right map shows the location and number of the sentient-3B (S3B) virtual stations.

Originating from the Tibetan Plateau, the Lancang and Nu Rivers flow through three provinces in China: Qinghai, Tibet, and Yunnan, and they flow out of the country from Yunnan Province. The Lancang River basin (21.15° – 33.82° N, 93.88° – 101.85° E) and the Nu River basin (23.10° – 32.76° N, 91.15° – 100.23° E) are both strip-shaped, with a northwest–southeast trend and a watershed area of $167,400 \text{ km}^2$ [58,60] and $137,800 \text{ km}^2$ [57,59], respectively. The length and area of the Lancang River account for 44.28% and 20.67% of its international river (Mekong River) [58,60], while those in Nu River account for 62.13% and 42.40% of its international river (Salween River) [57,59], respectively. The average elevation drops between the Lancang and Nu River are 2.12‰ and 2.04‰, respectively, with an average annual runoff volume of 76 and 70.3 billion km^3 , respectively.

The main channels of both rivers run nearby and share nearly identical geographic conditions, flowing at an altitude of over 5000 m in their origins to their respective estuaries [62]. However, while the Nu River remains pristine without human-made reservoirs or hydropower stations, the Lancang River basin contains 11 reservoirs [63]. The construction of water facilities significantly impacts the seasonal variation of WSE. So, the VSs in the two river basins allow us to evaluate the performance of Sentinel-3 over different terrains with different human impacts.

2.2. Data

2.2.1. Sentinel-3 Level-2 Data

The Copernicus Open Access Hub (<https://scihub.copernicus.eu/>, accessed on 11 October 2022) offers free registration and access to various types of Sentinel-3 data, including Level-1B, Level-2 land, and Level-2 water data. For this study, we used Level-2 land data that were processed as standard 20 Hz parameters data using OCOG retracking. These data provide the 20 Hz altimetric height above the reference ellipsoid and have undergone rigorous correction for different types of errors, including instrumental errors, range correction, and geophysical corrections such as dry and wet troposphere, ionosphere, solid earth tide, and polar tide [12,64,65].

2.2.2. Closed-Loop Tracking Command (CLTC) and Open-Loop Tracking Command (OLTC)

Sentinel-3A (S3A) started operating in closed-loop tracking command on 18 April 2016 (Figure 2 and Table A1). This mode comprises two operational steps: first, detection of useful signals and initialization of the tracker's range window, and second, tracking the echo's leading point to ensure it falls within the range window, typically in the middle third of the window [12,31]. However, this command faces difficulties in measuring the water surface elevation of rivers surrounded by or adjacent to steep slopes. In other words, for closed-loop detection of small and medium-sized rivers in mountainous areas, errors in the range window placement position may cause the echo not to be captured, resulting in erroneous or even invalid measurement data [11,65].

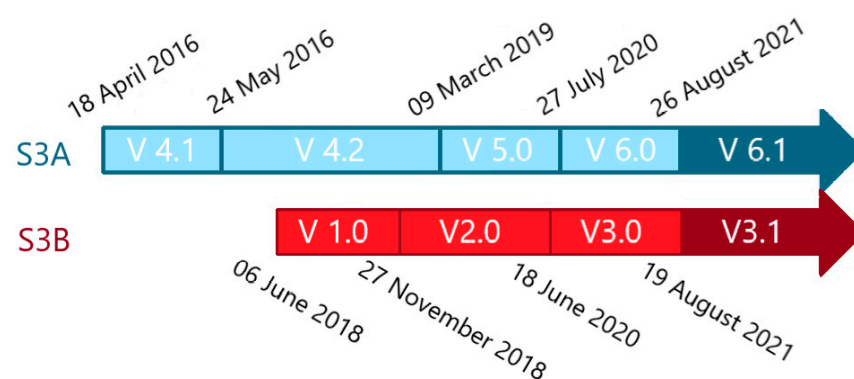


Figure 2. OLTC versions of Sentinel-3A (S3A) and Sentinel-3B (S3B) over time. The version number is indicated by the number in the arrow, while the time of the version change is provided at the top or bottom of the arrow (courtesy of <https://www.altimetry-hydro.eu/>, accessed on 6 August 2022).

Remote sensing technology has enabled the development of a satellite operation mode called OLTC (<https://www.altimetry-hydro.eu/>, accessed on 6 August 2022), which can enhance the efficiency and accuracy of the satellite [66]. OLTC works by focusing on virtual stations (VSs), which are surface points in the rivers of interest to researchers, instead of all water surface that the satellite can detect to improve its effectiveness [26,65]. The number of VSs and coverage of OLTC vary across different versions, as shown in Figure 2.

In March 2019, Sentinel-3 adopted OLTC from 60°S to 60°N, which allowed for the accurate location of the altimeter range window using OLTC tables without requiring shipboard sensors to capture signals (Figure 2). To generate OLTC tables, a pseudo-DEM was initially created using a global surface mask with a 300 m resolution provided by ACE2DEM and the given VSs. Due to the shipboard memory limitation, S3A and Sentinel-3B (S3B) can only accommodate up to 130,000 VSs each in OLTC tables.

During the tandem phase, both S3A and S3B used the same OLTC table (OLTC V4.2), but the S3B operated alternately between open-loop mode and closed-loop mode during the phase (the specific mode variation in S3B refers to [46]). After S3B reached its final orbit on 27 November 2018, an updated version 2.0 of the OLTC table was activated, increasing

the number of VSs to 32,515. This version was built specifically for S3B using an extended hydrological database. On 9 March 2019, the OLTC table for S3A was updated to version 5.0, increasing the number of VSs to 33,261.

New versions of the OLTC tables for S3B and S3A were released on 18 June and 27 July 2020, denoted as OLTC 3.0 and 6.0, respectively. These updates included more than twice the number of targets identified, particularly for rivers and lakes located above 60°N latitude, and corrected some incorrect values that were present in OLTC V5.0.

Further updates were made on 19 and 26 August 2021, resulting in versions 3.1 and 6.1 for S3B and S3A, respectively. The main focus of these updates was to improve the reference elevations of hydrographic targets 1262 (S3A) and 1153 (S3B) and to correct some incorrect values that were present in the OLTC tables. The placement of the VSs and the accuracy of the pseudo-DEM are critical factors that determine data quality, particularly when the number of VSs is limited in the future.

2.2.3. Other Data

In our study, we employed the water occurrence map developed by Pekel et al. [67] to ensure that the sampling areas contained water. These maps were created by analyzing over 3 million Landsat satellite images taken between 1984 and 2015, which enabled the identification of seasonal and annual changes in global surface water occurrence at a high resolution of 30 m, including the probability of water presence. To identify rivers, we selected a conservative threshold of 10% of water occurrences [12]. A low threshold is chosen on purpose to ensure all valuable data, including seasonal water, is extracted at the cost of a higher outlier frequency. This ensures that data points are not masked out because of low water occurrence probability, which could be partly due to cloud cover.

The ALOS (Advanced Land Observing Satellite), also known as Daichi, is an earth observation satellite program launched by Japan in 2006. The main purpose of this program is to collect global high-resolution land observation data for scientific research and commercial use. The free 12.5 m resolution DEM image used in this paper is from the PALSAR instrument of ALOS satellite. The altitude elevation of some VSs could not be determined for they did not receive effective echoes. ALOS data were chosen as a reference in this study to evaluate the performance of VSs at different altitudes.

3. Methodology

3.1. Methods Overview

As depicted in Figure 3, the methodology employed in this study can be summarized as follows: Initially, we obtained the location information of VSs by intersecting the Sentinel-3 Level-2 data with the water occurrence map at a 10% occurrence. Next, we generated a new waveform by computing the median values for multiple sampling points at each VS, and applied a range integrated power (RIP) threshold test ($RIP > 2000$) to identify the presence of water surface information [12]. Furthermore, we assessed the placement of the range window by analyzing the different gate positions of the waveform peaks. Subsequently, we compared the data quality of different VSs in closed-loop mode, open-loop mode, and various OLTC versions, and created a WSE time series for each VS. Finally, we compared the performance of the Sentinel-3 data for the Nu and Lancang Rivers and demonstrated the relationship between seasonal water level fluctuations and data quality using the example of cascade reservoirs.

3.2. Virtual Stations Extracting

A VS is defined as the intersection between a river line and a satellite ground track. To establish the location of virtual stations (VSs), we obtained the location information of VSs by intersecting the Sentinel-3 Level-2 data with the water occurrence map at a 10% occurrence. All VSs located on the main streams and assigned with OLTC are selected.

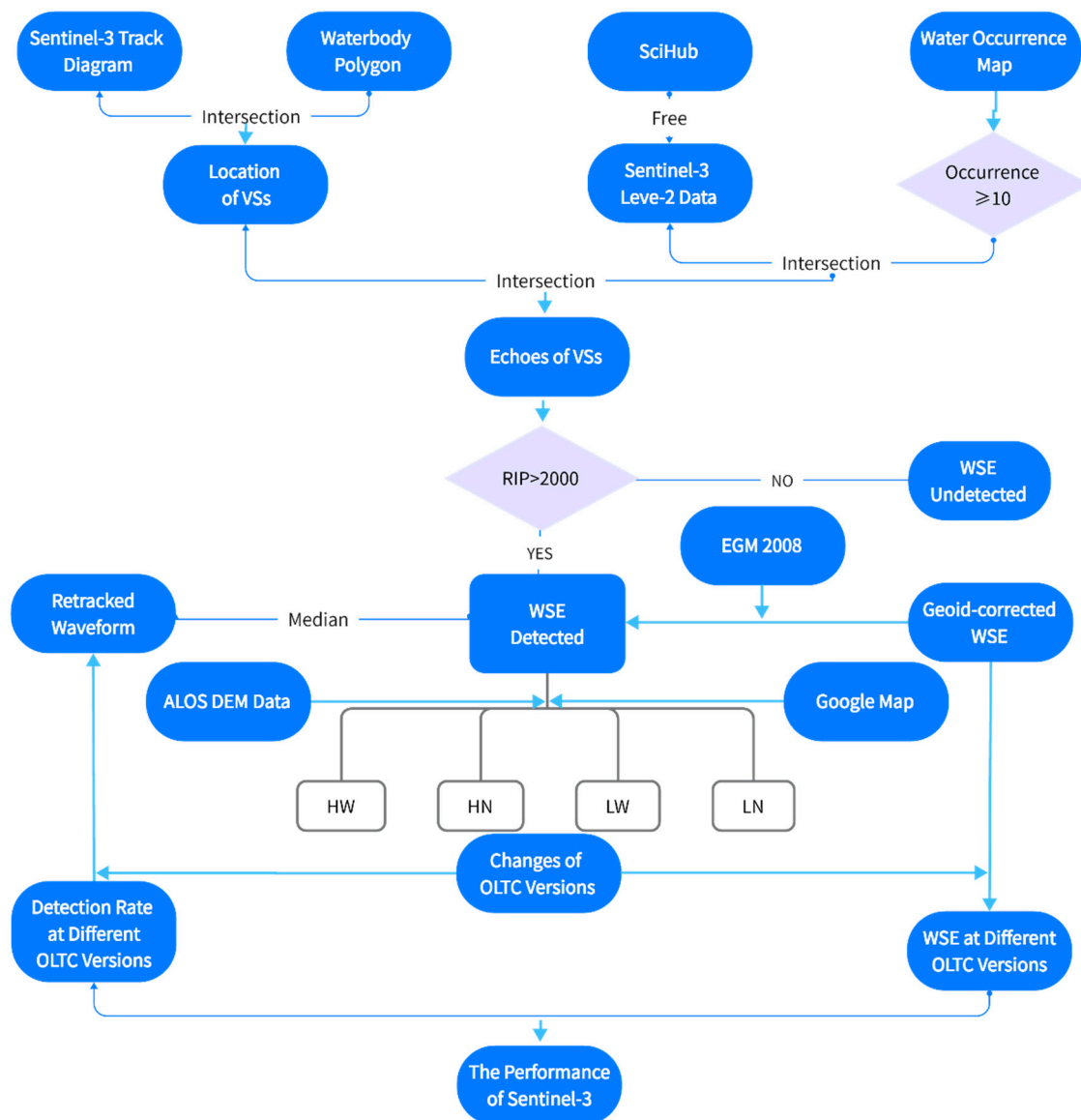


Figure 3. Research methodology flowchart.

3.3. Water Surface Elevation Detecting

Microwave pulses emitted by the altimeter are reflected by the water surface and recorded as partial echoes, as illustrated in Figure 4. To effectively detect echoes from the water surface, the receiving window must be accurately positioned, usually with a width of 60 m [68]. When the range window is centered on the water surface, as in Figure 4b, the maximum water surface fluctuation can be detected. However, if the range window is placed too high (Figure 4e) or too low (Figure 4d), the water surface will not be in the window, and the received echo peaks will be much lower than 2000, leading to noise or no echo at all, respectively [26]. Consequently, the information carried by the echoes of the VSs will not contribute to the monitoring of WSE, and these cases are defined as Undetected.

Conversely, if the range window is placed on the upper (Figure 4a) or lower (Figure 4c) side of the water surface, the water surface can still be detected, but the received echo peaks will be at the edge of the range bin window. This results in the inability to detect WSE accurately when the water level fluctuates at the sampling point. However, when only extreme river levels are of interest, the data from these cases can still provide reference values of WSE [69], and therefore, WSE data obtained from the above three range bin placements are considered as detected.

In the closed-loop period, the detection capability of the satellite is primarily influenced by the geographic influence rather than the satellite hardware facilities [46,51]. Once the satellite detects the water surface at a specific elevation, it retains the ability to detect the water surface at that elevation again in the closed-loop mode [12,25,46]. Therefore, if the satellite detects RIP > 2000 echoes at the VSs at least once during the closed-loop period, we deem the satellite's data to be reliable and define them as detected. This definition facilitates a more accurate comparison with the open-loop data.

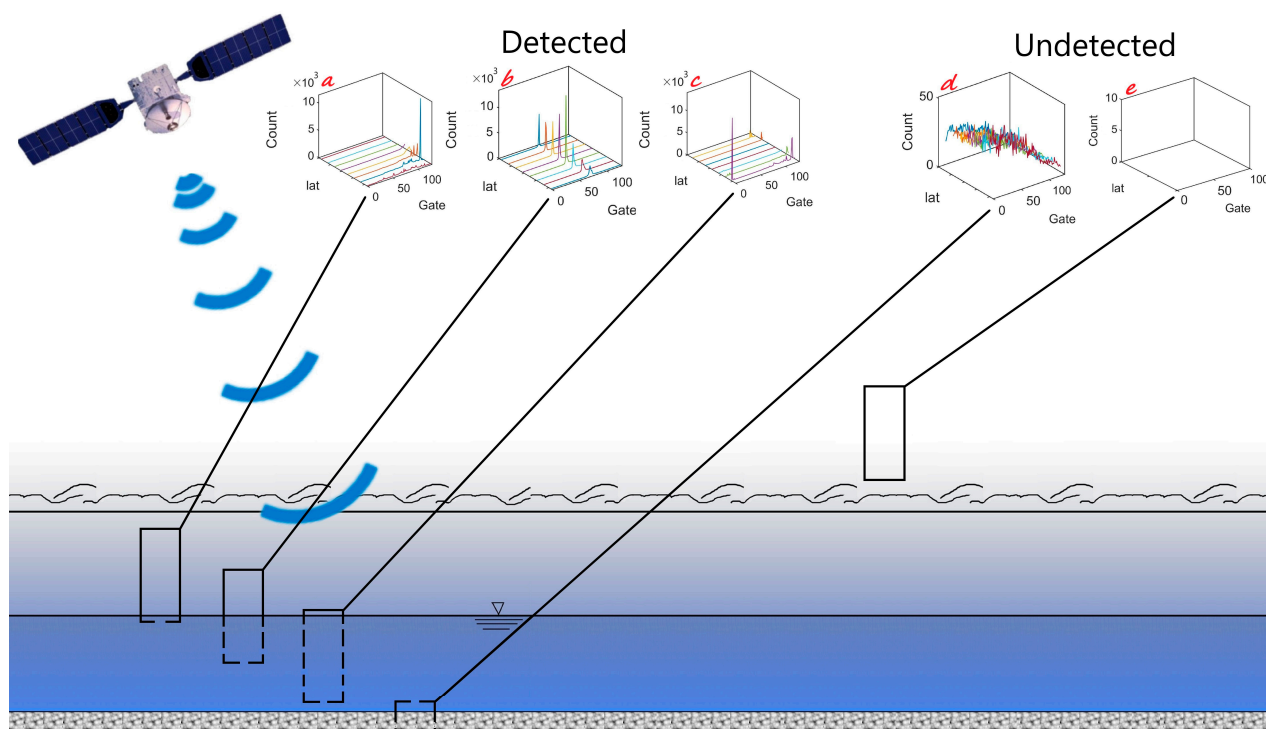


Figure 4. Satellite detection of water surface schematic. The first three (a–c) waveform graphs refer to the range window placed on the upper (a), in the middle (b) and on the lower (c) side of the water surface, respectively, and the water surface can be detected. The last two (d,e) waveform graphs refer to the range window placed too high (e) and too low (d), and the water surface cannot be detected. The black rectangles connected to the waveform graphs represent the range window, where the upper part of the water surface is represented by solid line while the lower part is represented by dashed line.

3.4. Elevation and Track Length Partitioning

In order to assess the performance of Sentinel-3 in various scenarios, the VSs were classified into four categories based on their elevation and track length: high elevation and wide river (HW), low elevation and wide river (LW), high elevation and narrow river (HN), and low elevation and narrow river (LN), using an elevation threshold of 2400 m and a track length of 500 m. The track length was determined by the intersection of the Sentinel-3 ground track and Google map [25,70]. Since the length of the intersection line in the study area is less than 3 km and the accuracy of the water occurrence picture is 30 m, the effect of Earth's gravity on the water surface can be neglected, and the water surface can be approximated as a smooth plane. Therefore, the length of the intersection line represents the distance that the satellite sweeps over the water body.

3.5. Time Series of WSE Constructing

To obtain the WSE from the Sentinel-3 Level-2b data, we need to calculate it by the following equation:

$$H = H_{\text{sat}} - \frac{S_{\text{wave}}}{2}$$

where H_{sat} is the satellite elevation, and S_{wave} is the distance the wave travels back and forth. H is the water surface height.

However, the wave propagation speed varies greatly in different media, temperatures, and densities, so the wave travel distance should be corrected for geophysical and propagation effects (i.e., pole tides, solid Earth tides, ionosphere, and dry and wet troposphere). The formula is modified to the following:

$$S_{\text{wave}} = vt - S_{\text{geo}}$$

where v is the wave speed, t is the time it takes for the wave to travel from emission to reception, and S_{geo} is the distance that needs to be increased or decreased by geographic condition correction.

The obtained water surface altitude is established based on the vehicle altitude, while WSE is the elevation of the water surface, so compared to WSE, H also needs to be corrected about the geodetic level:

$$WSE = H - H_{\text{geiod}}$$

Based on the above principles, we established the time series of WSE. For multiple observations at the same time, we first remove outliers based on water occurrence and backscatter coefficients, and then select the median value as the detection value. The specific data processing steps are referred to [11,25,70].

4. Results

4.1. Performance of S3A and S3B in Closed-Loop Mode and Different OLTC Versions

The performance of Sentinel-3 data for WSE is determined not only by the altimeter's tracking capability and resolution, but also by the accuracy of the OLTC table (Figure 2). This study gathered statistical comparisons to assess the quality of WSE detection during various periods, ranging from the closed-loop to open-loop mode. To this end, the study compared the echo results of S3A and S3B against a total of 66 VSs (38 for S3A and 28 for S3B, which are listed in Tables A2 and A3). The findings revealed that only three VSs in S3A could detect the water surface in any complete hydrological year from closed-loop to OLTC V6.1, with a probability of 7.9% (see Tables 1 and A4), whereas the probability of valid monitoring data in the closed-loop mode was 36.8% (see Table 1).

The detection rate of WSE improved considerably after entering the open-loop mode: it increased to 47.4% in OLTC V5.0 (launched in March 2019), 60.5% in OLTC V6.0 (launched in July 2020), and 63.2% in OLTC V6.1 (launched in August 2021) for S3A (see Table 1). For S3B, the probability of a stable detection rate was 46.4%, while the detection rate was 64.3% in OLTC V2.0 (launched in November 2018), 71.4% in OLTC V3.0 (launched in November 2018), and 75.0% in OLTC V3.1 (launched in August 2021) (see Table 1).

In total, only 25 out of 38 VSs in S3A, while 23 out of 28 VSs in S3B had valid data. As a result, the data validity probability of S3A was 65.8% in the entire Lancang–Nu River basin, while that of S3B was 82.1% (see Table 1).

Table 1. Detection rate of Sentinel-3 in different scenarios. The numerator indicates the number of valid virtual stations (VSs), and the denominator indicates the total number of VSs for all assessments. The detection result rate is shown in parentheses. The HW, LW, NH, and LN represent VSs in high elevation and wide river, low elevation and wide river, high elevation and narrow river, and low elevation and narrow river, respectively.

Total	S3A 25/38 (65.8%)				S3B 23/28 (82.1%)			
Total	Stable 3/38 (7.9%)		Unstable 22/38 (57.9%)		Stable 13/28 (46.4%)		Unstable 10/28 (41.7%)	
	closed-loop	V5.0	V6.0	V6.1	V1.0	V2.0	V3.0	V3.1
Total	14/38 (36.8%)	18/38 (47.4%)	23/38 (60.5%)	24/38 (63.2%)	-	18/28 (64.3%)	20/28 (71.4%)	21/28 (75.0%)
HW	3/3 (100.0%)	3/3 (100.0%)	3/3 (100.0%)	3/3 (100.0%)	-	1/1 (100.0%)	1/1 (100.0%)	1/1 (100.0%)
HN	0/22 (0%)	7/22 (31.8%)	8/22 (36.4%)	9/22 (40.9%)	-	10/19 (52.6%)	11/19 (57.9%)	13/19 (68.4%)
LW	4/4 (100.0%)	0/4 (0.0%)	4/4 (100.0%)	4/4 (100.0%)	-	3/3 (100.0%)	3/3 (100.0%)	3/3 (100.0%)
LN	7/9 (77.8%)	8/9 (88.8%)	8/9 (88.8%)	8/9 (88.8%)	-	4/5 (80.0%)	5/5 (100.0%)	4/5 (80.0%)

Note. Stable: the WSE is detected in any hydrological year. Unstable: the WSE is detected in at least one hydrological year.

4.2. Performance of S3A and S3B under Different Track Length and Elevation Conditions

As detailed in Section 3.3, this study divides all VSs into four regions based on a 2400 m elevation and 500 m track length (see Tables A2 and A3). Within the HW region, all the four VSs are situated near the source of the Nu River (as shown in Figure 5a). These VSs are located near to a large lake with a diameter much greater than 500 m in the interior of the Tibetan Plateau, where the terrain is relatively flat. Therefore, a valid WSE was detected in both the closed-loop mode and various versions of the open-loop mode (as shown in Figure 5b–f). Additionally, Sentinel-3 collects a good sequence of seasonal changes in WSE in these VSs. In the HN region, there are a total of 41 VSs, with 22 belonging to S3A and 19 to S3B. However, due to the complex geography and high altitude in this region, waves from satellites can hardly touch the water surface, resulting in only 23 VSs receiving valid data, with 10 belonging to S3A and 13 to S3B. Among the 13 detected S3B VSs, only three VSs (NO. 47.2, NO. 218.4, and NO. 218.5) obtained a complete time series of WSE, as listed in Table A4. Moreover, none of the VSs detected valid WSE data during the closed-loop mode (Figure 5h). To illustrate the situation, a representative VS is shown in Figure 5g–i.

The LW area contained seven VSs, with four belonging to S3A and three to S3B. Among the three S3B VSs, the WSE could be detected in every version of the OLTC. For the four S3A VSs, the typical waveform changes were observed as shown in Figure 6b–f. During the closed-loop mode, these VSs exhibited a good performance and they were able to collect the complete WSE data. However, no valid echoes were received after the transition from the closed-loop mode to the open-loop mode (OLTC V5.0). The situation had changed completely in the OLTC V6.0 when all four VSs detected WSE perfectly again. The LN region contains 14 VSs, 9 of which belonging to S3A and 5 to S3B. Among the 14 stations, only NO. 4.2 of S3A was undetected, the other 13 VSs were detected with a good seasonal variation of WSE. The typical waveform changes are shown in Figure 6g–i.

Overall, the HN region had the lowest detection rate among the four study regions. Moreover, the open-loop mode outperformed the closed-loop mode at high altitudes (Figure 7), but the closed-loop mode performed better at low altitudes. This contrast is due to the water storage in the cascade reservoirs, which will be discussed in detail in Section 5.3.

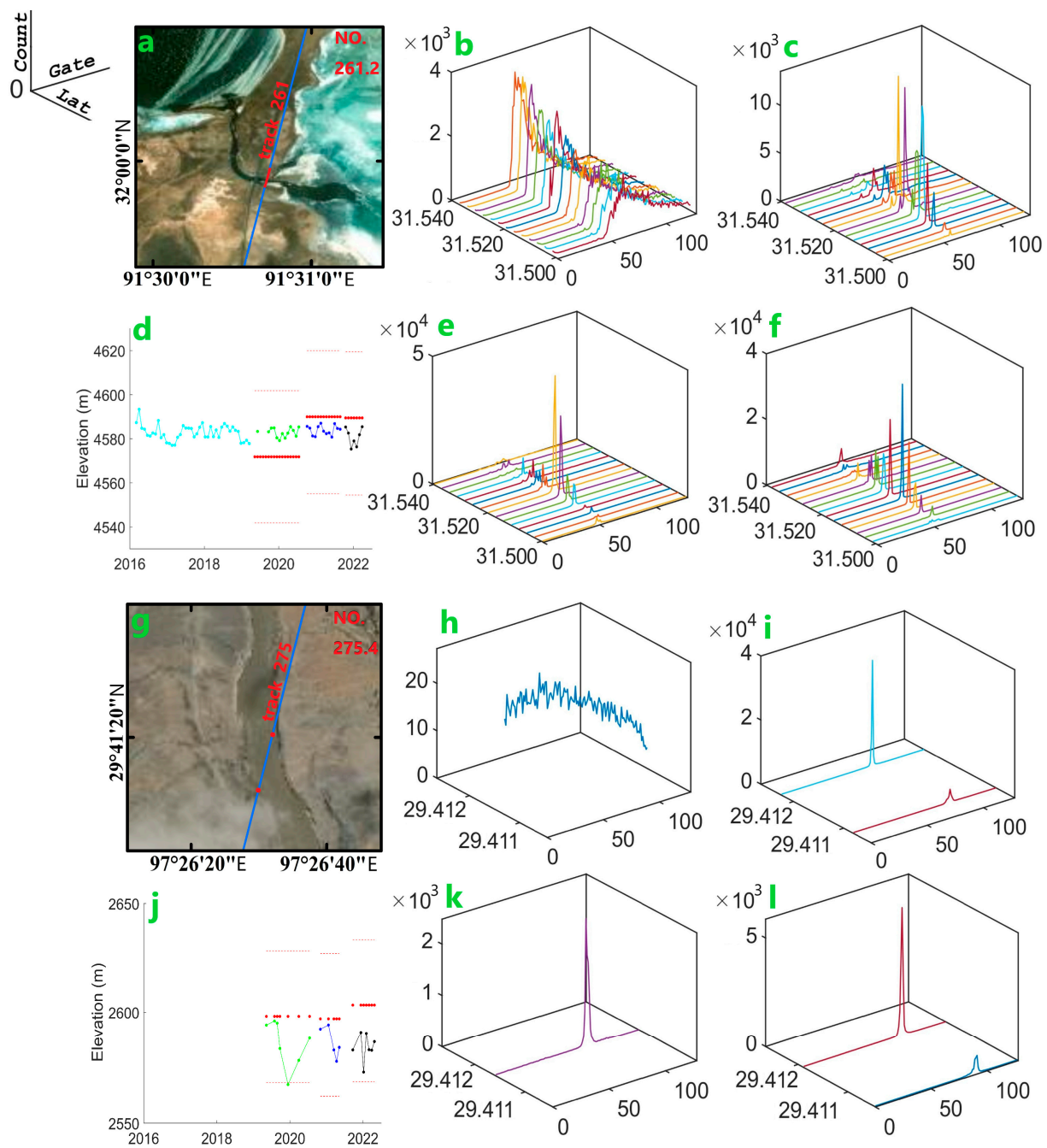


Figure 5. Two typical cases of virtual stations (VSs) in (a–f) high elevation and wide river (HW) and (g–l) high elevation and narrow river (HN). The satellite image shows the locations of the VSs, with the orbit of Sentinel-3A (S3A) indicated by the blue line. The orbit numbers are shown in red next to the orbit, and the red dots on the orbit indicate the location of the satellite emitting detection waves at the corresponding VSs. The VSs number is displayed in red font in the upper right corner of the image. The red dots in the scatter chart (d,j) represent the elevation of OLTC while the pink dots represent the size of the range window. The four waveforms refer to the closed-loop (b,h) and OLTC V5.0 (c,i), OLTC V6.0 (e,k), and OLTC V6.1 (f,l). (d,j) show the time series of the WSE for the specific VS, where azure, green, blue, and black refer to closed-loop, OLTC V5.0, OLTC V6.0, and OLTC V6.1.

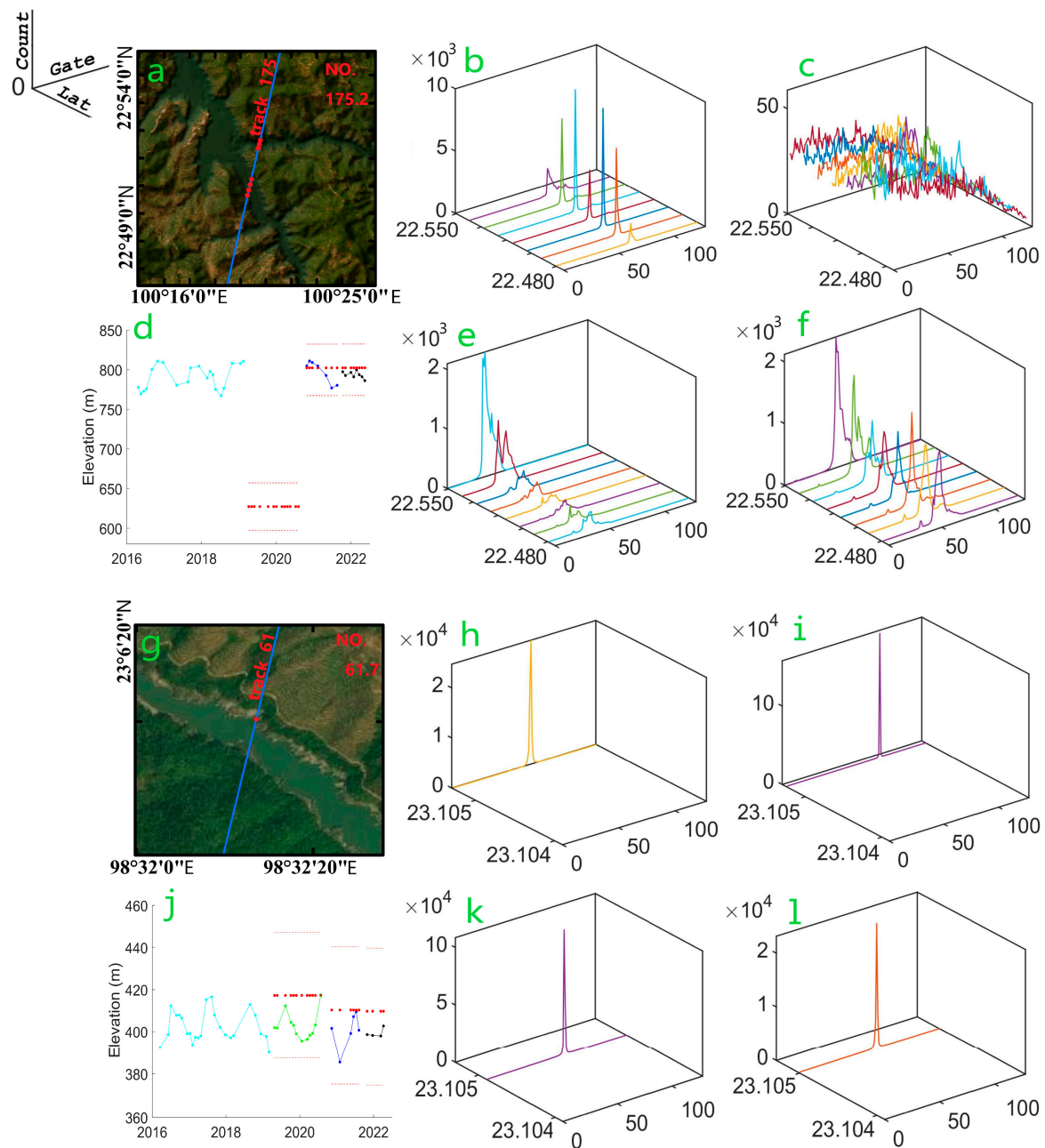


Figure 6. Two typical cases of virtual stations (VSs) in (a–f) low elevation and wide river (LW) and (g–l) low elevation and narrow river (LN). The satellite image shows the locations of the VSs, with the orbit of Sentinel-3A (S3A) indicated by the blue line. The orbit numbers are shown in red next to the orbit, and the red dots on the orbit indicate the location of the satellite emitting detection waves at the corresponding VSs. The VSs number is displayed in red font in the upper right corner of the image. The red dots in the scatter chart (d,j) represent the elevation of OLTC while the pink dots represent the size of the range window. The four waveforms refer to the closed-loop (b,h) and OLTC V5.0 (c,i), OLTC V6.0 (e,k), and OLTC V6.1 (f,l). (d,j) Show the time series of the WSE for the specific VS, where azure, green, blue, and black refer to closed-loop, OLTC V5.0, OLTC V6.0, and OLTC V6.1.

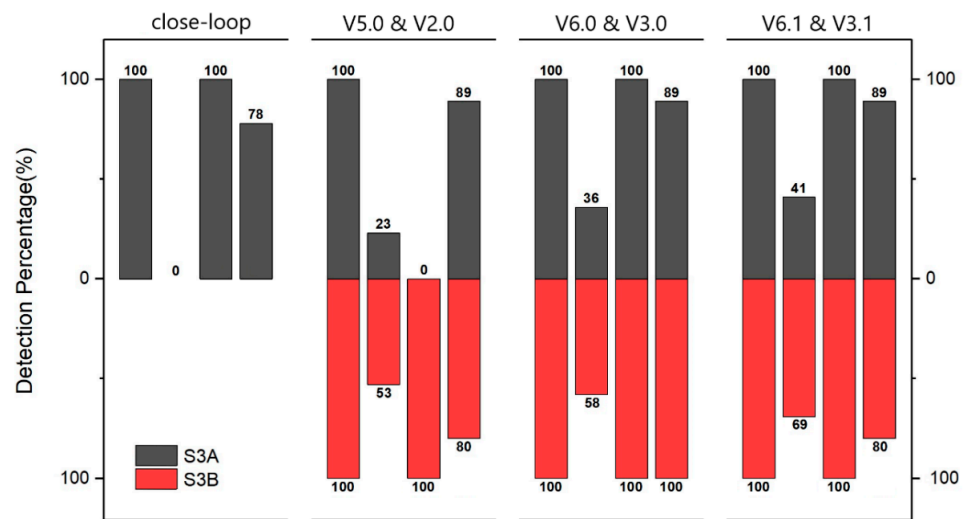


Figure 7. Comparison of the detection rates of Sentinel-3A (S3A) and Sentinel-3B (S3B) at different stages. The bars of each stage from left to right are the detection rate in the high elevation and wide river (HW), high elevation and narrow river (HN), low elevation and wide river (LW), and low elevation and narrow river (LN), respectively.

4.3. Performance of S3A and S3B in Lancang and Nu River Basins

As shown in Figure 8, the detection rate of S3A was much lower in the Nu River basin compared to the Lancang River basin, with 13.0% and 35.7% in the closed-loop mode, respectively. At the beginning of the open-loop mode (OLTC V5.0), the detection rate of S3A increased to 60.9% in the Nu River basin, while it decreased to 28.5% in the Lancang River basin. However, with the update of OLTC, the detection rates of S3A in both the Nu and Lancang River basins improved to 65.2% and 50.0%, and 65.2% and 57.1% in OLTC V6.0, and V6.1, respectively. The situation was different in S3B, for the detection rate in the Nu River basin was basically unchanged, while there was a small fluctuation in the Lancang River basin. The detection rates in both the Nu and Lancang River basins were 73.3% and 53.8%, 73.3% and 69.2%, and 86.7% and 61.5% in the OLTC V2.0, V3.0, and V3.1, respectively.

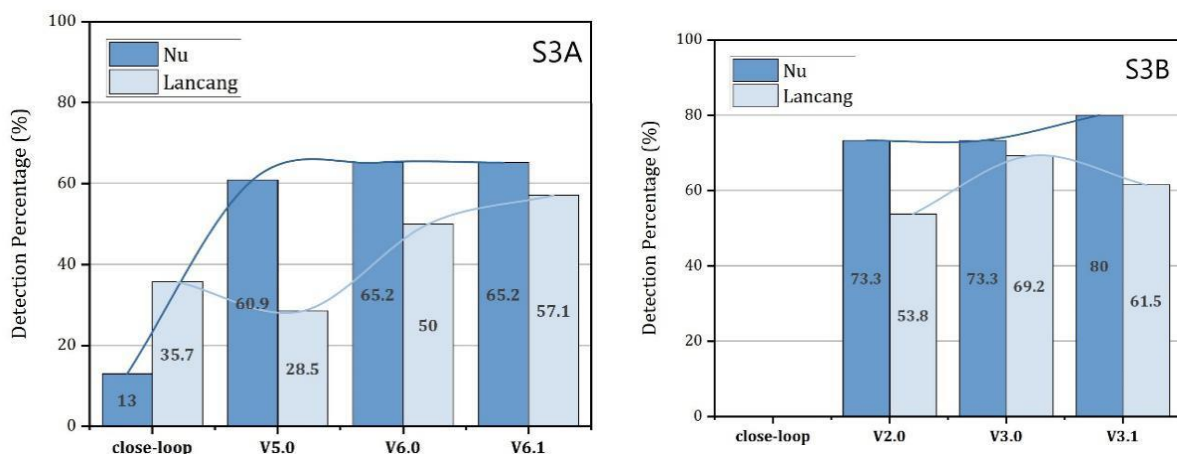


Figure 8. Comparison of the detection rates in the Lancang and Nu Rivers at different stages. The left panel of the figure displays the performance of Sentinel-3A (S3A), while the right panel shows that of Sentinel-3B (S3B). The bars and trend lines represent the satellite’s detection rate in the region and the trend line of the detection rate, respectively. The Nu River is denoted by the blue color, while the Lancang River is represented by the greenish-gray color.

5. Discussion

5.1. The Data Quality of S3A and S3B under Various Conditions

HW performed best in the WSE detection among the four regions, where all the stable VSs in S3A were situated. Due to its flat terrain, stable water recharge, little impact of human activities, and proximity to lakes within the Qinghai–Tibetan Plateau, the WSE was easily detected in the closed-loop mode. Moreover, as the birthplace of international rivers, the region has a strong hydrological research foundation, leading to the accurate placement of the range window in every period of the open-loop mode (unlike the misplacement of the range window in the reservoirs), allowing for the establishment of a complete time series of the WSE in both of the open-loop and closed-loop modes.

In the closed-loop mode, none of the VSs in the HN region could detect the WSE due to the high altitude, narrow water surface, and significant topographic relief surrounding the water bodies. However, one-third of them could do so at the beginning of the open-loop mode (OLTC V5.0), and the detection rate improved with the change in the OLTC versions (Figure 7). This indicated that the use of the open-loop mode and the proper placement of the range window significantly improved the detection rate of the WSE in high mountain rivers. Still, some VSs (e.g., NO. 61.7) were found to detect the WSE in the previous OLTC version, but failed to do so after the change in the OLTC table.

Clear seasonal patterns were captured in the Sentinel-3 WSE detection in the Zambezi basin by Kittel et al. [12], and the LW region shares the same geography. However, contrary to our expectation, after transition to the open-loop mode (Figure 9), the data quality of the VSs that performed well in the closed-loop mode decreased significantly. This situation occurred in four VSs located in the Lancang River basin reservoir areas, where the construction of reservoirs in recent years led to the expansion and rise of the water surface, resulting in the incorrect placement of the range window in OLTC V5.0 [26]. However, after OLTC was updated to V6.0, the situation improved as the range windows were repositioned to the correct positions and all four VSs could detect WSE again. However, changes in water volume, rather than WSE reference values, are of greater concern in the reservoir area, which requires a complete time series of WSE. However, according to echoes from the VSs in reservoir areas (Figure 10), the extreme values of WSE cannot be detected in the open-loop mode for the seasonal variations of water level exceeding the limit of the range window (usually 60 m). This renders the creation of a complete time series of WSE impossible.

The smooth water flow and flat terrain in the LN region provide favorable conditions for the WSE detection of Sentinel-3 to achieve a good performance in both of the closed-loop and open-loop modes. However, a similar situation occurred as in the HN region (e.g., NO. 61.7), where some VSs that could detect the WSE in previous OLTC versions (e.g., NO. 61.3) could not do so with the update of the OLTC table. Combining the information from the two regions, the incorrect OLTC update was the key for the situation. Moreover, for the narrow river surface and the fluctuating terrain in the two regions, the majority of the range window was not placed on the water surface all the time. Thus, the significant fluctuation of WSE in mountainous areas makes it possible for the WSE to exceed the range window for the entire time of the new OLTC (e.g., NO. 61.7).

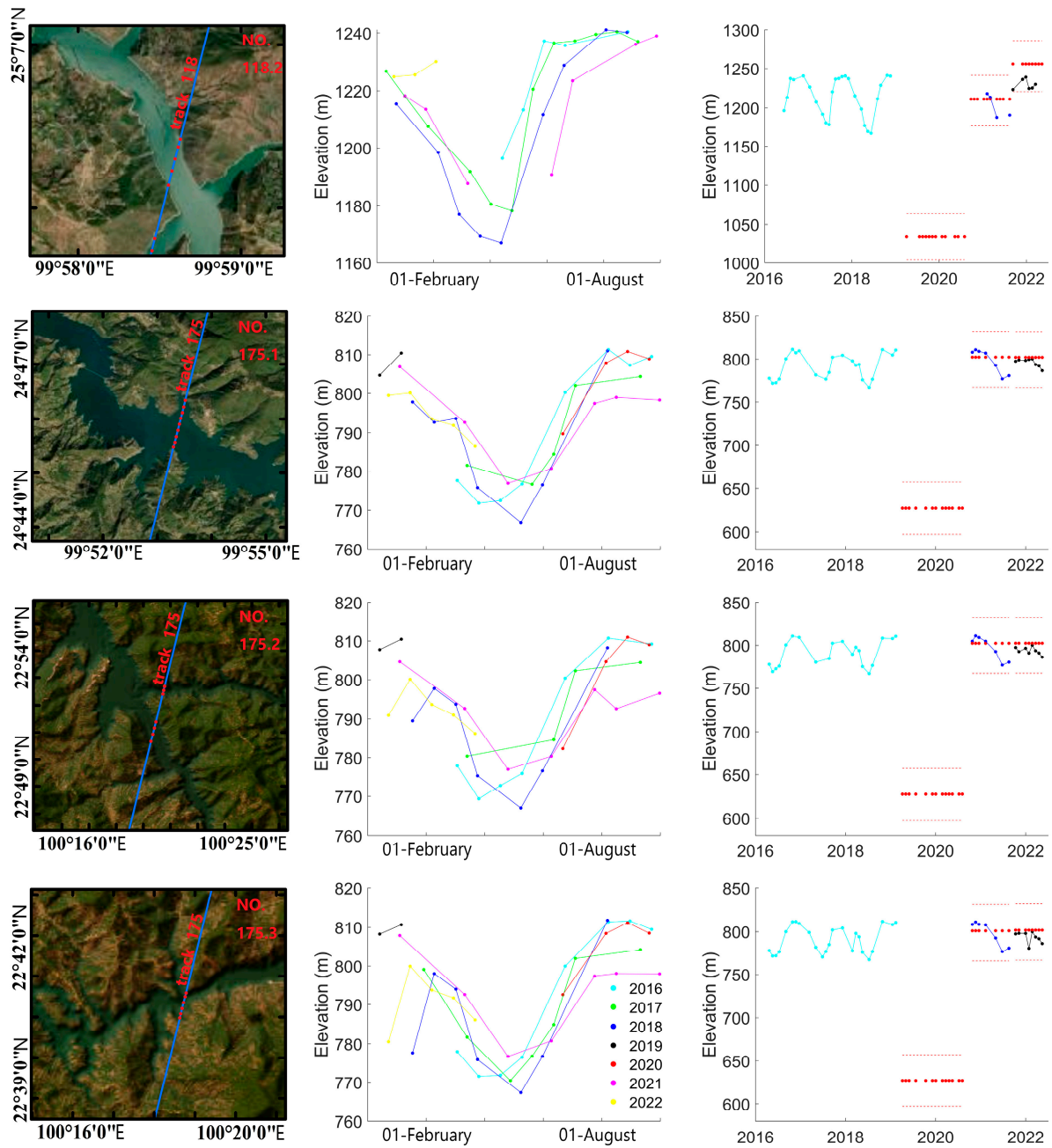


Figure 9. Four VSs in the reservoir areas. The satellite image shows the locations of the VSs, with the orbit of Sentinel-3A (S3A) indicated by the blue line. The orbit numbers are shown in red next to the orbit, and the red dots on the orbit indicate the location of the satellite emitting detection waves at the corresponding VSs. The VSs number is displayed in red font in the upper right corner of the image. The figure in the middle is the variation of WSE variation at the same time for different years. Figure in the right is show the time series of the WSE for the specific VS, where azure, green, blue, and black refer to closed-loop, OLTC V5.0, OLTC V6.0, and OLTC V6.1.

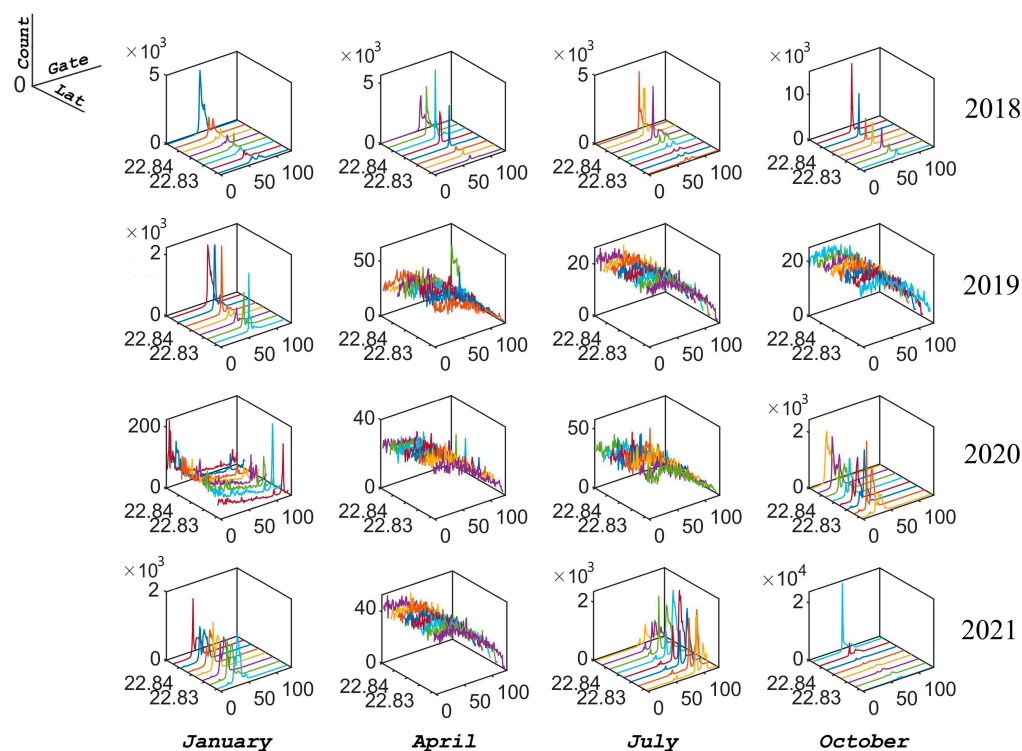


Figure 10. Echogram of NO. 175.1 virtual station arranged over time. The number on the right represents the year, and the word below represents the month.

5.2. Comparison of S3A and S3B in the Study Region

The detection rates from the research by Kittel et al. in the Zambezi River basin were 36.6%, 44.0%, and 48.8% in the closed-loop mode, OLTC V5.0, and OLTC V2.0, respectively [12], while the numbers in this study are 36.8%, 47.4%, and 64.3%, respectively (Table 1). The situation displays a significant improvement in the capability of the Sentinel-3 to detect water surface information as the transition from the closed-loop mode to the open-loop mode occurs. Moreover, the detection rate of S3A increased with the implementation of newer OLTC versions to 60.5% and 63.2% in OLTC V6.0 and V6.1, respectively, while the detection rate of S3B rose to 71.4% and 75.0% in OLTC V3.0 and V3.1, respectively, which is the same as the prediction by Jiang et al. [70]. However, the probability of stable was low for both S3A and S3B, particularly for S3A, which highlights the challenges of establishing a complete time series of WSE.

According to Taburet et al. [46], the difference in data availability between S3A and S3B during the tandem phase when they operated in different tracking modes was attributed to the closed-loop mode. This indicates that the two satellites have the same detection capability for WSE. However, it is clear that S3B outperforms S3A in WSE detection from Figure 8 and Table A4, and with their hardware differences excluded, the comparison of detection rates at reservoirs between OLTC V5.0 and V2.0 indicates that the OLTC settings for S3B are more precise than those for S3A. Additionally, observations of the VSs location in high mountainous areas suggests that several VSs in S3A were not appropriately placed on the water surface; some were even placed on the river bank adjacent to the water surface, whereas this was not the case for S3B. Moreover, the different tracks of S3A and S3B result in the different locations of their VSs, making the better geographical conditions in S3B possible for its better performance.

5.3. Impacts of Reservoirs Impoundment on S3A and S3B

The study by Zhang et al. [14] noted that the establishment of the cascade reservoirs widened the water surface of the Lancang River, which significantly improved the detection

rate of WSE during the closed-loop mode, helping it to have a better performance than that in the Nu River. However, due to the establishment of the cascade reservoirs, the WSE in the Lancang River basin changes rapidly while the OLTC table is not able to record this information in OLTC V5.0. The result was that the performance of Sentinel-3 in the Lancang River basin was lower than that in the Nu River basin in the OLTC V5.0, and not as good as itself in the closed-loop mode; these results are the same as those found by of Zhang et al. [26].

It is evident from Figure 8 that with the change in the OLTC versions, the detection rate of WSE in the Lancang River basin had a clear upward trend, while it was basically unchanged in the Nu River basin. After the comparison with different OLTC tables, it was found that the OLTC tables of most VSs were not detected with the change in the OLTC versions. So, the situation could be explained with the fact that multiple updates of OLTC coincidentally missed the correct values of the WSE in the Nu River basin. However, it is more likely due to the fact that improving the accuracy of the OLTC table is currently insignificant in comparison to increasing the detection rate of Sentinel-3 in the Nu River basin.

5.4. Advantages and Limitations in the Approach and Prospects for Future Research

Satellite radar altimetry has been widely used over the past few decades to bridge the gap between data requirements in hydrologic/hydrodynamic simulations and in situ data availability. The dual-satellite mission Sentinel-3 joins a new generation of satellites carrying high-resolution SAR altimeters, which outperforms previous radar altimetry missions in terms of time coverage and resolution. We explored the performance of Sentinel-3 altimetry over high mountain and cascade reservoirs basins by dividing it into four regions with different river widths and elevations. The study shows that the detection rate of Sentinel-3A and Sentinel-3B improves when transitioning from a closed-loop mode to an open-loop mode and with the implementation of newer OLTC versions. Additionally, Sentinel-3A performs better when detecting water surfaces in the Lancang River than the Nu River, due to the cascade reservoir causing river channel expansion.

Although the data covered the periods of abundance and depletion in V6.1 and V3.1, a complete hydrological year was not covered in these two OLTC versions. However, since the OLTC table has been updated to V6.2 and V3.2 on 8 and 15 September 2022, respectively, whether the update of the OLTC table has a significant improvement on the detection rate of Sentinel-3 needs to be studied in the future. Kittel et al. [12] believed that the success is entirely dependent on the accuracy of the OLTC tables, as data are missing from the S3A records, which is in large part due to the latency between the mission start and OLTC update. Now, Sentinel-3 allows all to propose amendments to the OLTC table at <https://www.altimetry-hydro.eu/>, which effectively avoids incomplete revisions to the OLTC table and reduces the delay in OLTC updates. Additionally, this study treats VSs with echo energies greater than 2000 as identified to the water surface, but nearby bright targets such as small lakes and ponds could be a source of errors for Sentinel-3 [12,25]. Although it had been confirmed through satellite images that there were no bright targets nearby, the state of a certain moment cannot exclude the disturbance.

The detection ability of Sentinel-3 is improving with the implementation of newer OLTC versions, but seasonal variations of water levels in reservoirs exceeding the size of the range window may render a complete measurement impossible. As the seasonal variation of the WSE in reservoirs (more than 100 m [13]) usually exceeds the range window (usually 60 m), the WSE in reservoirs cannot be detected completely over a hydrological year in the open-loop mode. Here, two solutions are proposed to address hardware issues and enable the Sentinel-3 to capture the complete annual variation of WSE in reservoirs. The first solution involves setting up multiple VSs within a reservoir and adjusting the OLTC of each VS according to the fluctuations in WSE. By adding more groups of VSs, the range window could be extended to cover the maximum WSE fluctuations. For example, by setting a reservoir with two groups of VSs, we can theoretically identify up to 120 m of

water level fluctuations in the reservoirs. The second solution involves dividing the VSs into several sets of OLTCs based on the expected water level fluctuations in the reservoirs. During the period of abundant water, the OLTC table with a higher value would be used, and in the dry period, a lower range window would be placed. This real-time OLTC update would enable more accurate monitoring of the WSE in the study area.

6. Conclusions

This study aimed to evaluate the effectiveness of S3A and S3B in detecting the WSE in high mountain areas, plains, and reservoir areas using the Lancang and Nu River basins as examples. The main findings are as follows:

1. Transitioning from the closed-loop mode to the open-loop mode and upgrading to newer OLTC versions improved the detection rates for both S3A (from 36.8% in closed-loop to 47.4%, 60.5%, and 63.2% in OLTC V5.0, V6.0, and V6.1, respectively) and S3B (from 64.3% in OLTC V2.0 to 71.4% and 75.0% in OLTC V3.0 and V3.1, respectively) in both the Lancang and Nu River basins.
2. The updated OLTC version significantly improved the data quality of VSs in high mountain and narrow rivers, except for a few VSs. Compared to the initial satellite launch, the detection rate improved by 40.9% for S3A and 15.8% for S3B.
3. The closed-loop model of S3A performed better when detecting the WSE in the Lancang River than in the Nu River at lower elevations due to the impoundment of cascade reservoirs, which extended the water surface width of the Lancang River. However, in OLTC V5.0, S3A had difficulty detecting the effective data in the lower reaches of the Lancang River because the elevation of the reservoir water surface resulted in a range window that was too low. This problem has since been addressed by OLTC V6.0 due to the correct placement of the range window.
4. In the Lancang River basin, the seasonal variations of the WSE in reservoirs that exceed 60 m may exceed the range window size (60 m), making a complete measurement impossible despite improvements in the OLTC versions.

This study provides valuable insights into the performance of S3A and S3B in detecting WSE in different types of landscapes and under various conditions, and a reference value on the performance of Sentinel-3 for mountainous areas, plains, and reservoir areas of water surface elevation detection after OLTC V5.0. The study also identifies some limitations of the current OLTC technology. The prospect of this study lies in the potential application of Sentinel-3 in monitoring water resources in mountainous regions, which are crucial for many downstream communities and ecosystems. This study provides a useful reference for future research concerning the improvement of remote sensing technology and the monitoring of water resources in challenging environments.

Author Contributions: Y.C.: methodology, software, writing—original draft. X.Z.: conceptualization, methodology, software, writing—original draft. Z.Y.: conceptualization, methodology, writing—original draft. All authors contributed to the article. All authors have read and agreed to the published version of the manuscript.

Funding: The research was financially supported by the Strategic Priority Research Program of the Chinese Academy of Sciences (Grants No. XDA2006020202), the National Natural Science Foundation of China (Grants No. 42201037), and the project was funded by China Postdoctoral Science Foundation (Grants No. 2022M713122). Xingxing Zhang was financially supported by the Chinese Scholarship Council, the Special Research Assistant Program of the Chinese Academy of Sciences (Grant No. E2S20001Y5), which is gratefully acknowledged.

Data Availability Statement: Sentinel-3 data are publicly accessible at <https://scihub.copernicus.eu/dhus/> (accessed on 11 October 2022); Google map data are publicly accessible at <https://www.google.com> (accessed on 11 October 2022); and ALOS DEM data are publicly accessible at <https://earth.esa.int/eogateway/missions/alos> (accessed on 11 October 2022).

Conflicts of Interest: The authors declare that they have no known competing financial interest or personal relationships that could have appeared to influence the work reported in this paper.

Appendix A

Table A1. Description of successive open-loop tracking command (OLTC) versions on Sentinel-3A and Sentinel-3B.

Mission	OLTC Version	Date of Activation	Number of VSs	VSs' Type:		Update Changes
				Rivers/Lakes/Reservoirs/Glaci	ers	
Sentinel-3A	V4.1	18 April 2016	2253	2007/246/-/-		-
	V4.2	24 May 2016	2253	2007/246/-/-		4 areas of interest between 25°N and 60°N in the open-loop
	V5.0	9 March 2019	33,261	17,409/14,427/1,386/39		31,008 VSs were added between 60° S and 60°N
	V6.0	27 July 2020	74,050	20,100/47,637/4,262/51		40,798 VSs were added in the world
	V6.1	26 August 2021	74,050	20,100/47,637/4,262/51		reference elevations of 1262 VSs were improved
Sentinel-3B	V1.0 (tandem)	6 June 2018	2253	2007/246/-/-		-
	V2.0	27 November 2018	32,515	17,016/14,245/1,231/23		32515 VSs were added in the 60° S–60°N
	V3.0	18 June 2020	73,629	21,719/47,738/4,149/23		41,114 VSs were added in the world
	V3.1	19 August 2021	73,629	21,719/47,738/4,149/23		reference elevations of 1153 were improved

Table A2. Information on virtual stations in S3A for this study, including station number, track length (estimated from Google Earth), elevation (estimated from ALOS), and coordinates.

Station	Detected or Not	Track Length (m)	Elevation (m)	Location	Lon (°)	Lat (°)
4.3	Detected	110	1398	Nu	98.76	27.62
47.1	Detected	80	3769	Nu	94.20	31.48
61.2	Detected	510	1304	Lancang	99.22	25.79
61.3	Detected	270	652	Nu	98.95	24.75
61.5	Detected	280	453	Nu	98.61	23.40
61.6	Detected	340	434	Nu	98.57	23.23
61.7	Detected	370	410	Nu	98.54	23.11
61.8	Detected	230	408	Nu	98.52	23.05
61.9	Detected	230	397	Nu	98.51	22.98
104.5	Detected	120	3452	Nu	95.04	31.16
118.1	Detected	80	1239	Lancang	99.98	25.11
118.2	Detected	120	1272	Lancang	99.88	24.76
175.1	Detected	1080	812	Lancang	100.34	22.84
175.2	Detected	880	769	Lancang	100.35	22.86
175.3	Detected	840	795	Lancang	100.30	22.66
261.1	Detected	1880	4596	Nu	91.58	32.15
261.2	Detected	1620	4597	Nu	91.55	32.05
261.3	Detected	1540	4591	Nu	91.51	31.92
275.2	Detected	100	3022	Lancang	97.65	30.44
275.4	Detected	190	2587	Nu	97.44	29.69
318.1	Detected	380	4405	Nu	92.31	31.44
318.2	Detected	200	4400	Nu	92.28	31.33
332.5	Detected	150	2605	Lancang	98.35	29.58
332.7	Detected	120	2093	Nu	98.15	28.86
375.2	Detected	190	4049	Nu	93.27	31.53
4.2	Undetected	80	1914	Lancang	98.89	28.13
61.4	Undetected	110	559	Nu	98.80	24.13
104.2	Undetected	110	3991	Lancang	95.51	32.86
104.3	Undetected	150	4126	Lancang	95.41	32.46
104.4	Undetected	40	3575	Nu	95.08	31.31
104.6	Undetected	70	4117	Nu	94.93	30.77
161.3	Undetected	110	3707	Lancang	96.33	32.44
161.4	Undetected	120	3713	Lancang	96.18	31.90
161.5	Undetected	80	3226	Nu	95.92	30.95
218.4	Undetected	80	3443	Lancang	97.07	31.72
218.5	Undetected	120	3357	Lancang	96.95	31.31
218.6	Undetected	120	3021	Nu	96.69	30.37
375.1	Undetected	40	4191	Nu	93.45	32.17

Table A3. Information on virtual stations in S3B for this study, including station number, track length (estimated from Google Earth), elevation (estimated from ALOS), and coordinates.

Station	Detected or Not	Track Length (m)	Elevation (m)	Location	Lon (°)	Lat (°)
4.3	Detected	80	2230	Lancang	98.64	28.94
4.4	Detected	290	1723	Nu	98.47	28.31
47.1	Detected	40	3914	Nu	93.80	31.73
47.2	Detected	120	3893	Nu	93.73	31.48
61.3	Detected	60	1631	Lancang	99.11	27.19
61.4	Detected	340	950	Nu	98.88	26.28
61.5	Detected	150	924	Nu	98.87	26.27
104.1	Detected	40	4160	Lancang	95.09	33.00
104.2	Detected	80	3591	Nu	94.60	31.24
118.2	Detected	1200	1228	Lancang	99.51	25.12
118.3	Detected	350	495	Nu	99.13	23.62
161.3	Detected	40	3835	Lancang	95.90	32.56
161.4	Detected	80	3913	Lancang	95.78	32.13
161.5	Detected	110	3363	Nu	95.47	31.04
175.1	Detected	1280	989	Lancang	100.35	24.75
175.2	Detected	1350	807	Lancang	99.97	23.23
218.3	Detected	80	3580	Lancang	96.71	32.11
218.4	Detected	80	3541	Lancang	96.59	31.67
218.5	Detected	190	3125	Nu	96.35	30.81
275.3	Detected	120	3316	Lancang	97.29	30.83
275.4	Detected	110	2734	Nu	97.11	30.17
332.2	Detected	110	2834	Lancang	98.01	30.06
375.1	Detected	80	4173	Nu	92.84	31.64
375.2	Detected	40	4189	Nu	92.81	31.53
275.2	Undetected	110	3165	Lancang	97.33	30.99
318.1	Undetected	120	4498	Nu	91.83	31.39
332.3	Undetected	50	3765	Nu	97.89	29.62
332.4	Undetected	50	2392	Nu	97.83	29.40

Table A4. Detection rate of each component, including stable, unstable, HW, HN, LW, LN, and different versions of OLTC.

	S3A			S3B				
	Closed-Loop	V5.0	V6.0	V6.1	V2.0	V3.0	V3.1	
4.3		✓	✓	✓	4.3	✓	✓	✓
47.1		✓	✓	✓	4.4	✓	✓	✓
61.2		✓	✓	✓	47.1	✓	✓	✓
61.3		✓	✓	✓	47.2	✓	✓	✓
61.5		✓	✓	✓	61.3	✓	✓	✓
61.6		✓	✓	✓	61.4	✓	✓	✓
61.7		✓	✓	✓	61.5	✓	✓	✓
61.8		✓	✓	✓	104.1	✓	✓	✓
61.9		✓	✓	✓	104.2	✓	✓	✓
104.5		✓	✓	✓	118.2	✓	✓	✓
118.1		✓	✓	✓	118.3	✓	✓	✓
118.2	✓		✓	✓	161.3			✓
175.1	✓		✓	✓	161.4	✓	✓	✓
175.2	✓		✓	✓	161.5	✓	✓	✓
175.3	✓		✓	✓	175.1	✓	✓	✓
261.1	✓	✓	✓	✓	175.2	✓	✓	✓
261.2	✓	✓	✓	✓	218.3	✓	✓	✓
261.3	✓	✓	✓	✓	218.4	✓	✓	✓
275.2		✓	✓	✓	218.5	✓	✓	✓
275.4		✓	✓	✓	275.3			✓
318.1			✓	✓	275.4	✓		✓
318.2			✓	✓	332.2		✓	
332.5		✓	✓	✓	375.1	✓		
332.7		✓	✓	✓	375.2	✓	✓	✓
375.2		✓	✓	✓				

Note. ✓ indicates that a valid water body information is detected.

References

1. Kleinherenbrink, M.; Lindenbergh, R.C.; Ditmar, P.G. Monitoring of lake level changes on the Tibetan Plateau and Tian Shan by retracking Cryosat SARIn waveforms. *J. Hydrol.* **2015**, *521*, 119–131. [[CrossRef](#)]
2. Nielsen, K.; Stenseng, L.; Andersen, O.B.; Villadsen, H.; Knudsen, P. Validation of CryoSat-2 SAR mode based lake levels. *Remote Sens. Environ.* **2015**, *171*, 162–170. [[CrossRef](#)]
3. Chen, T.; Song, C.; Zhan, P.; Fan, C. Densifying and Optimizing the Water Level Series for Large Lakes from Multi-Orbit ICESat-2 Observations. *Remote Sens.* **2023**, *15*, 780. [[CrossRef](#)]
4. Tian, B.; Gao, P.; Mu, X.; Zhao, G. Water Area Variation and River–Lake Interactions in the Poyang Lake from 1977–2021. *Remote Sens.* **2023**, *15*, 600. [[CrossRef](#)]
5. Kandekar, V.U.; Pande, C.B.; Rajesh, J.; Atre, A.A.; Gorantiwar, S.D.; Kadam, S.A.; Gavit, B. Surface water dynamics analysis based on sentinel imagery and Google Earth Engine Platform: A case study of Jayakwadi dam. *Sustain. Water Resour. Manag.* **2021**, *7*, 44. [[CrossRef](#)]
6. Domeneghetti, A.; Tarpanelli, A.; Brocca, L.; Barbetta, S.; Moramarco, T.; Castellarin, A.; Brath, A. The use of remote sensing-derived water surface data for hydraulic model calibration. *Remote Sens. Environ.* **2014**, *149*, 130–141. [[CrossRef](#)]
7. Ahmed, R.; Rawat, M.; Wani, G.F.; Ahmad, S.T.; Ahmed, P.; Jain, S.K.; Meraj, G.; Mir, R.A.; Rather, A.F.; Farooq, M. Glacial Lake Outburst Flood Hazard and Risk Assessment of Gangabal Lake in the Upper Jhelum Basin of Kashmir Himalaya Using Geospatial Technology and Hydrodynamic Modeling. *Remote Sens.* **2022**, *14*, 5957. [[CrossRef](#)]
8. Yin, Z.; Li, X.; Huang, C.; Chen, W.; Hou, B.; Li, X.; Han, W.; Hou, P.; Han, J.; Ren, C.; et al. Analysis of the Formation Mechanism of Medium and Low-Temperature Geothermal Water in Wuhan Based on Hydrochemical Characteristics. *Water* **2023**, *15*, 227. [[CrossRef](#)]
9. Hu, W.-F.; Yao, J.-Q.; He, Q.; Yang, Q. Spatial and temporal variability of water vapor content during 1961–2011 in Tianshan Mountains, China. *J. Mt. Sci.* **2015**, *12*, 571–581. [[CrossRef](#)]
10. Wongchuig-Correa, S.; de Paiva, R.C.D.; Biancamaria, S.; Collischonn, W. Assimilation of future SWOT-based river elevations, surface extent observations and discharge estimations into uncertain global hydrological models. *J. Hydrol.* **2020**, *590*, 125473. [[CrossRef](#)]
11. Jiang, L.; Nielsen, K.; Andersen, O.B.; Bauer-Gottwein, P. Monitoring recent lake level variations on the Tibetan Plateau using CryoSat-2 SARIn mode data. *J. Hydrol.* **2017**, *544*, 109–124. [[CrossRef](#)]
12. Kittel, C.M.M.; Jiang, L.; Tøttrup, C.; Bauer-Gottwein, P. Sentinel-3 radar altimetry for river monitoring—A catchment-scale evaluation of satellite water surface elevation from Sentinel-3A and Sentinel-3B. *Hydrol. Earth Syst. Sci.* **2021**, *25*, 333–357. [[CrossRef](#)]
13. Sichangi, A.W.; Wang, L.; Yang, K.; Chen, D.; Wang, Z.; Li, X.; Zhou, J.; Liu, W.; Kuria, D.; Naturvetenskapliga, F.; et al. Estimating continental river basin discharges using multiple remote sensing data sets. *Remote Sens. Environ.* **2016**, *179*, 36–53. [[CrossRef](#)]
14. Zhang, X.; Jiang, L.; Liu, Z.; Kittel, C.M.; Yao, Z.; Druce, D.; Wang, R.; Tøttrup, C.; Liu, J.; Jiang, H.; et al. Flow regime changes in the Lancang River, revealed by integrated modeling with multiple Earth observation datasets. *Sci. Total. Environ.* **2023**, *862*, 160656. [[CrossRef](#)]
15. Lobera, G.; Besné, P.; Vericat, D.; López-Tarazón, J.; Tena, A.; Aristi, I.; Díez, J.; Ibasate, A.; Larrañaga, A.; Elosegi, A.; et al. Geomorphic status of regulated rivers in the Iberian Peninsula. *Sci. Total. Environ.* **2015**, *508*, 101–114. [[CrossRef](#)]
16. Blöschl, G. Three hypotheses on changing river flood hazards. *Hydrol. Earth Syst. Sci.* **2022**, *26*, 5015–5033. [[CrossRef](#)]
17. Debnath, J.; Sahariah, D.; Lahon, D.; Nath, N.; Chand, K.; Meraj, G.; Farooq, M.; Kumar, P.; Kanga, S.; Singh, S.K. Geospatial modeling to assess the past and future land use-land cover changes in the Brahmaputra Valley, NE India, for sustainable land resource management. *Environ. Sci. Pollut. Res.* **2022**, *ahead of print*. [[CrossRef](#)]
18. Hardeng, J.; Bakke, J.; Sabatier, P.; Støren, E.W.N.; Van der Bilt, W. Lake sediments from southern Norway capture Holocene variations in flood seasonality. *Quat. Sci. Rev.* **2022**, *290*, 107643. [[CrossRef](#)]
19. Hannah, D.M.; DeMuth, S.; van Lanen, H.A.J.; Looser, U.; Prudhomme, C.; Rees, G.; Stahl, K.; Tallaksen, L.M. Large-scale river flow archives: Importance, current status and future needs. *Hydrol. Process.* **2011**, *25*, 1191–1200. [[CrossRef](#)]
20. Schneider, C.; Flörke, M.; De Stefano, L.; Petersen-Perlman, J.D. Hydrological threats to riparian wetlands of international importance—A global quantitative and qualitative analysis. *Hydrol. Earth Syst. Sci.* **2017**, *21*, 2799–2815. [[CrossRef](#)]
21. Thu, H.N.; Wehn, U. Data sharing in international transboundary contexts: The Vietnamese perspective on data sharing in the Lower Mekong Basin. *J. Hydrol.* **2016**, *536*, 351–364. [[CrossRef](#)]
22. Hiep, N.H.; Luong, N.D.; Ni, C.-F.; Hieu, B.T.; Huong, N.L.; Du Duong, B. Factors influencing the spatial and temporal variations of surface runoff coefficient in the Red River basin of Vietnam. *Environ. Earth Sci.* **2023**, *82*, 56. [[CrossRef](#)]
23. Li, Y.; Li, B.; Yuan, Y.; Lei, Q.; Jiang, Y.; Liu, Y.; Li, R.; Liu, W.; Zhai, D.; Xu, J. Trends in total nitrogen concentrations in the Three Rivers Headwater Region. *Sci. Total. Environ.* **2022**, *852*, 158462. [[CrossRef](#)]
24. Zhong, R.; Zhao, T.; Chen, X.; Jin, H. Monitoring drought in ungauged areas using satellite altimetry: The Standardized River Stage Index. *J. Hydrol.* **2022**, *612*, 128308. [[CrossRef](#)]
25. Jiang, L.; Nielsen, K.; Dinardo, S.; Andersen, O.B.; Bauer-Gottwein, P. Evaluation of Sentinel-3 SRAL SAR altimetry over Chinese rivers. *Remote Sens. Environ.* **2020**, *237*, 111546. [[CrossRef](#)]

26. Zhang, X.; Jiang, L.; Kittel, C.M.M.; Yao, Z.; Nielsen, K.; Liu, Z.; Wang, R.; Liu, J.; Andersen, O.B.; Bauer-Gottwein, P. On the Performance of Sentinel-3 Altimetry Over New Reservoirs: Approaches to Determine Onboard A Priori Elevation. *Geophys. Res. Lett.* **2020**, *47*, e2020GL088770. [[CrossRef](#)]
27. Arsen, A.; Crétaux, J.-F.; Del Rio, R.A. Use of SARAL/AltiKa over Mountainous Lakes, Intercomparison with Envisat Mission. *Mar. Geodesy* **2015**, *38*, 534–548. [[CrossRef](#)]
28. Biancamaria, S.; Frappart, F.; Leleu, A.-S.; Mariieu, V.; Blumstein, D.; Desjonquères, J.-D.; Boy, F.; Sottolichio, A.; Valle-Levinson, A. Satellite radar altimetry water elevations performance over a 200 m wide river: Evaluation over the Garonne River. *Adv. Space Res.* **2017**, *59*, 128–146. [[CrossRef](#)]
29. Jiang, M.; Behrens, P.; Wang, T.; Zhipeng, T.; Yu, Y.; Chen, D.; Liu, L.; Ren, Z.; Zhou, W.; Zhu, S.; et al. Provincial and sector-level material footprints in China. *Proc. Natl. Acad. Sci. USA* **2019**, *116*, 26484–26490. [[CrossRef](#)] [[PubMed](#)]
30. Boergens, E.; Nielsen, K.; Andersen, O.B.; Dettmering, D.; Seitz, F. River Levels Derived with CryoSat-2 SAR Data Classification—A Case Study in the Mekong River Basin. *Remote Sens.* **2017**, *9*, 1238. [[CrossRef](#)]
31. Chelton, D.B.; Esbensen, S.K.; Schlax, M.G.; Thum, N.; Freilich, M.H.; Wentz, F.J.; Gentemann, C.L.; McPhaden, M.J.; Schopf, P.S. Observations of coupling between surface wind stress and sea surface temperature in the eastern tropical Pacific. *J. Clim.* **2001**, *14*, 1479–1498. [[CrossRef](#)]
32. Chelton, D.B.; Freilich, M.H.; Johnson, J.R. Evaluation of Unambiguous Vector Winds from the Seasat Scatterometer. *J. Atmos. Ocean. Technol.* **1989**, *6*, 1024–1039. [[CrossRef](#)]
33. Wingham, D.; Francis, C.; Baker, S.; Bouzinac, C.; Brockley, D.; Cullen, R.; de Chateau-Thierry, P.; Laxon, S.; Mallow, U.; Mavrocordatos, C.; et al. CryoSat: A mission to determine the fluctuations in Earth's land and marine ice fields. *Nat. Hazards Oceanogr. Process. Satell. Data* **2006**, *37*, 841–871. [[CrossRef](#)]
34. Frappart, F.; Legrésy, B.; Niño, F.; Blarel, F.; Fuller, N.; Fleury, S.; Birol, F.; Calmant, S. An ERS-2 altimetry reprocessing compatible with ENVISAT for long-term land and ice sheets studies. *Remote Sens. Environ.* **2016**, *184*, 558–581. [[CrossRef](#)]
35. Berry, P.A.M.; Garlick, J.D.; Freeman, J.A.; Mathers, E.L. Global inland water monitoring from multi-mission altimetry. *Geophys. Res. Lett.* **2005**, *32*, 22814. [[CrossRef](#)]
36. Normandin, C.; Frappart, F.; Diepkilé, A.T.; Mariieu, V.; Mougin, E.; Blarel, F.; Lubac, B.; Braquet, N.; Ba, A. Evolution of the Performances of Radar Altimetry Missions from ERS-2 to Sentinel-3A over the Inner Niger Delta. *Remote Sens.* **2018**, *10*, 833. [[CrossRef](#)]
37. Dawson, G.; Landy, J.; Tsamados, M.; Komarov, A.S.; Howell, S.; Heorton, H.; Krumpfen, T. A 10-year record of Arctic summer sea ice freeboard from CryoSat-2. *Remote Sens. Environ.* **2022**, *268*, 112744. [[CrossRef](#)]
38. Morris, A.; Moholdt, G.; Gray, L.; Schuler, T.V.; Eiken, T. CryoSat-2 interferometric mode calibration and validation: A case study from the Austfonna ice cap, Svalbard. *Remote Sens. Environ.* **2021**, *269*, 112805. [[CrossRef](#)]
39. Nilsson, B.; Andersen, O.B.; Ranndal, H.; Rasmussen, M.L. Consolidating ICESat-2 Ocean Wave Characteristics with CryoSat-2 during the CRYO2ICE Campaign. *Remote Sens.* **2022**, *14*, 1300. [[CrossRef](#)]
40. Chen, P.; An, Z.; Xue, H.; Yao, Y.; Yang, X.; Wang, R.; Wang, Z. INPPTR: An improved retracking algorithm for inland water levels estimation using Cryosat-2 SARin data. *J. Hydrol.* **2022**, *613*, 128439. [[CrossRef](#)]
41. Kleinherenbrink, M.; Naeije, M.; Slobbe, C.; Egido, A.; Smith, W. The performance of CryoSat-2 fully-focussed SAR for inland water-level estimation. *Remote Sens. Environ.* **2020**, *237*, 111589. [[CrossRef](#)]
42. Li, P.; Li, H.; Chen, F.; Cai, X. Monitoring Long-Term Lake Level Variations in Middle and Lower Yangtze Basin over 2002–2017 through Integration of Multiple Satellite Altimetry Datasets. *Remote Sens.* **2020**, *12*, 1448. [[CrossRef](#)]
43. Heorton, H.; Tsamados, M.; Armitage, T.; Ridout, A.; Landy, J. CryoSat-2 Significant Wave Height in Polar Oceans Derived Using a Semi-Analytical Model of Synthetic Aperture Radar 2011–2019. *Remote Sens.* **2021**, *13*, 4166. [[CrossRef](#)]
44. Lian, T.; Xin, X.; Peng, Z.; Li, F.; Zhang, H.; Yu, S.; Liu, H. Estimating Evapotranspiration over Heterogeneous Surface with Sentinel-2 and Sentinel-3 Data: A Case Study in Heihe River Basin. *Remote Sens.* **2022**, *14*, 1349. [[CrossRef](#)]
45. Shen, M.; Duan, H.; Cao, Z.; Xue, K.; Qi, T.; Ma, J.; Liu, D.; Song, K.; Huang, C.; Song, X. Sentinel-3 OLCI observations of water clarity in large lakes in eastern China: Implications for SDG 6.3.2 evaluation. *Remote Sens. Environ.* **2020**, *247*, 111950. [[CrossRef](#)]
46. Taburet, N.; Zawadzki, L.; Vayre, M.; Blumstein, D.; Le Gac, S.; Boy, F.; Raynal, M.; Labroue, S.; Crétaux, J.-F.; Femenias, P. S3MPC: Improvement on Inland Water Tracking and Water Level Monitoring from the OLTC Onboard Sentinel-3 Altimeters. *Remote Sens.* **2020**, *12*, 3055. [[CrossRef](#)]
47. Wan, Y.; Zhang, R.; Pan, X.; Fan, C.; Dai, Y. Evaluation of the Significant Wave Height Data Quality for the Sentinel-3 Synthetic Aperture Radar Altimeter. *Remote Sens.* **2020**, *12*, 3107. [[CrossRef](#)]
48. Vu, D.T.; Dang, T.D.; Galelli, S.; Hossain, F. Satellite observations reveal 13 years of reservoir filling strategies, operating rules, and hydrological alterations in the Upper Mekong River basin. *Hydrol. Earth Syst. Sci.* **2022**, *26*, 2345–2364. [[CrossRef](#)]
49. Zhang, C.; Lv, A.; Zhu, W.; Yao, G.; Qi, S. Using Multisource Satellite Data to Investigate Lake Area, Water Level, and Water Storage Changes of Terminal Lakes in Ungauged Regions. *Remote Sens.* **2021**, *13*, 3221. [[CrossRef](#)]
50. Biancamaria, S.; Schaedele, T.; Blumstein, D.; Frappart, F.; Boy, F.; Desjonquères, J.-D.; Pottier, C.; Blarel, F.; Niño, F. Validation of Jason-3 tracking modes over French rivers. *Remote Sens. Environ.* **2018**, *209*, 77–89. [[CrossRef](#)]
51. Martin-Puig, C.; Leuliette, E.; Lillibridge, J.; Roca, M. Evaluating the Performance of Jason-2 Open-Loop and Closed-Loop Tracker Modes. *J. Atmos. Ocean. Technol.* **2016**, *33*, 2277–2288. [[CrossRef](#)]

52. Yuan, J.; Guo, J.; Niu, Y.; Zhu, C.; Li, Z.; Liu, X. Denoising Effect of Jason-1 Altimeter Waveforms with Singular Spectrum Analysis: A Case Study of Modelling Mean Sea Surface Height over South China Sea. *J. Mar. Sci. Eng.* **2020**, *8*, 426. [[CrossRef](#)]
53. Abdalla, S. Are Jason-2 significant wave height measurements still useful. *Adv. Space Res.* **2021**, *68*, 802–807. [[CrossRef](#)]
54. Vignudelli, S.; Cipollini, P.; Gommenginger, C.; Gleason, S.; Snaith, H.M.; Coelho, H.; Fernandes, M.J.; Lázaro, C.; Nunes, A.L.; Gómez-Enri, J.; et al. Satellite Altimetry: Sailing Closer to the Coast. *Remote Sens. Chang. Ocean.* **2011**, 217–238. [[CrossRef](#)]
55. Steunou, N.; Picot, N.; Sengenès, P.; Noubel, J.; Frery, M. AltiKa Radiometer: Instrument Description and In-Flight Performance. *Mar. Geodesy* **2015**, *38*, 43–61. [[CrossRef](#)]
56. Le Gac, S.; Boy, F.; Blumstein, D.; Lasson, L.; Picot, N. Benefits of the Open-Loop Tracking Command (OLTC): Extending conventional nadir altimetry to inland waters monitoring. *Adv. Space Res.* **2021**, *68*, 843–852. [[CrossRef](#)]
57. Yang, Y.; Weng, B.; Yan, D.; Niu, Y.; Dai, Y.; Li, M.; Gong, X. Partitioning the contributions of cryospheric change to the increase of streamflow on the Nu River. *J. Hydrol.* **2021**, *598*, 126330. [[CrossRef](#)]
58. Zhong, X.; Li, J.; Wang, J.; Zhang, J.; Liu, L.; Ma, J. Linear and Nonlinear Characteristics of Long-Term NDVI Using Trend Analysis: A Case Study of Lancang-Mekong River Basin. *Remote Sens.* **2022**, *14*, 6271. [[CrossRef](#)]
59. Jiang, J.; Zhu, S.; Wang, W.; Li, Y.; Li, N. Coupling coordination between new urbanisation and carbon emissions in China. *Sci. Total. Environ.* **2022**, *850*, 158076. [[CrossRef](#)]
60. Tian, F.; Hou, S.; Morovati, K.; Zhang, K.; Nan, Y.; Lu, X.X.; Ni, G. Exploring spatio-temporal patterns of sediment load and driving factors in Lancang-Mekong River basin before operation of mega-dams (1968–2002). *J. Hydrol.* **2023**, *617*, 128922. [[CrossRef](#)]
61. Xu, X.; Zhang, X.; Li, X.; Henry, A.J. Evaluation of the Applicability of Three Methods for Climatic Spatial Interpolation in the Hengduan Mountains Region. *J. Hydrometeorol.* **2023**, *24*, 35–51. [[CrossRef](#)]
62. Yuan, X.; Wang, J.; He, D.; Lu, Y.; Sun, J.; Li, Y.; Guo, Z.; Zhang, K.; Li, F. Influence of cascade reservoir operation in the Upper Mekong River on the general hydrological regime: A combined data-driven modeling approach. *J. Environ. Manag.* **2022**, *324*, 116339. [[CrossRef](#)] [[PubMed](#)]
63. Sun, Z.; Sun, L.; Zheng, H.; Li, Z. Estimation of sedimentation in the Manwan and Jinghong reservoirs on the Lancang river. *Water Supply* **2022**, *22*, 4307–4319. [[CrossRef](#)]
64. Lizundia-Loiola, J.; Franquesa, M.; Khairoun, A.; Chuvieco, E. Global burned area mapping from Sentinel-3 Synergy and VIIRS active fires. *Remote Sens. Environ.* **2022**, *282*, 113298. [[CrossRef](#)]
65. Windle, A.E.; Evers-King, H.; Loveday, B.R.; Ondrusek, M.; Silsbe, G.M. Evaluating Atmospheric Correction Algorithms Applied to OLCI Sentinel-3 Data of Chesapeake Bay Waters. *Remote Sens.* **2022**, *14*, 1881. [[CrossRef](#)]
66. Desjonquères, J.D.; Carayon, G.; Steunou, N.; Lambin, J. Poseidon-3 Radar Altimeter: New Modes and In-Flight Performances. *Mar. Geodesy* **2010**, *33*, 53–79. [[CrossRef](#)]
67. Pekel, J.-F.; Cottam, A.; Gorelick, N.; Belward, A.S. High-resolution mapping of global surface water and its long-term changes. *Nature* **2016**, *540*, 418–422. [[CrossRef](#)]
68. Michailovsky, C.I.; McEnnis, S.; Berry, P.A.M.; Smith, R.; Bauer-Gottwein, P. River monitoring from satellite radar altimetry in the Zambezi River basin. *Hydrol. Earth Syst. Sci.* **2012**, *16*, 2181–2192. [[CrossRef](#)]
69. Wang, J.; Tang, Q.; Yun, X.; Chen, A.; Sun, S.; Yamazaki, D. Flood inundation in the Lancang-Mekong River Basin: Assessing the role of summer monsoon. *J. Hydrol.* **2022**, *612*, 128075. [[CrossRef](#)]
70. Jiang, L.; Nielsen, K.; Andersen, O.B.; Bauer-Gottwein, P. CryoSat-2 radar altimetry for monitoring freshwater resources of China. *Remote Sens. Environ.* **2017**, *200*, 125–139. [[CrossRef](#)]

Disclaimer/Publisher’s Note: The statements, opinions and data contained in all publications are solely those of the individual author(s) and contributor(s) and not of MDPI and/or the editor(s). MDPI and/or the editor(s) disclaim responsibility for any injury to people or property resulting from any ideas, methods, instructions or products referred to in the content.